

ALE3D Simulations of Laser Melting Stainless Steel

Zhigang Wu

RadiaSoft, LLC, 3380 Mitchell Ln, Boulder, CO

May 06, 2019

Abstract

The ALE3D code has been employed to study energy beam processing metals in additive manufacturing. In this study we focused on laser melting bulk steel (stainless 316L), investigating the relations between melt hole geometry (hole width, hole depth, and the width-to-depth ratio) and parameters for laser (power, size, scanning speed, etc.) and those for steel's optical properties (absorptivity, extinction coefficient). We find that our present simulated results agree well with both experimental data and previous ALE3D results. This investigation paves the way for reliable ALE3D simulations of electron-beam processing metallic powder materials.

Keywords: Additive manufacturing, finite element analysis, ALE3D, laser, electron beam, heat transfer, melting, stainless steel, powder bed fusion.

1. Motivations

The emergence of powder bed metal additive manufacturing (AM [2]) has enabled many new strategies in AM research and engineering, due to the benefits of reduced number of sub-assemblies, shortened lead-time, increased part quality, and reduced administrative costs. Compared with laser-based metal AM, interests in the electron-beam (e-beam) is growing rapidly. However, these AM processes, especially e-beam powder bed fusion (EB-PBF), represents emergent complexity as the interactions between powder metallurgy, beam optics, heat transfer, rapid solidification and microstructure evolution determine the properties of the final workpiece. Large thermal gradients and enormous residue stress are often incurred in AM processes, making direct measurements extremely difficult and resulting in cracking and/or delamination.

Researchers and engineers usually employ a trial-and-error approach, which is expensive and time-consuming, since the manufactured parts have to be built many times until the quality of the product becomes acceptable. Thus, reliable finite element modeling (FEM) of AM processes plays an increasingly crucial role in this research area. The well calibrated FEM results provide the capability for feed-forward process, leading to optimized build strategies and accelerated part development and certification.

In this preliminary study we have focused on employing the ALE3D code [3] to carry out the FEM of laser heating and melting bulk stainless steel (316L). The main purpose is to demonstrate that we are able to simulate intense laser beam irradiating the surface of metal over the length scale of a few tens of μm . Once this specific FEM is well tested against previous simulations and experiments, it is straightforward to carry out the ALE3D simulations of e-beam processing bulk metals and metallic powder materials, if no extra complexity, such as keyhole formation, is present.

2. Methods and Parameters for ALE3D Simulations

Energy absorption and temperature distribution in heated metals are simulated using the Multiphysics ALE3D code, which takes advantage of the arbitrary Lagrangian (mesh moves with the material) Eulerian (mesh is fixed in space)—ALE—techniques, using a hybrid finite element and finite volume formulation to address a wide range of materials problems on an unstructured grid. Large mesh distortions are addressed

via mesh relaxation and/or the ALE techniques [4], in which material is advected through the mesh, and advection is implemented in a Lagrangian plus remap scheme.

Theoretical Approach

Temperature distribution in both bulk metals and powder metallic materials as a function of time is simulated based on a transient thermal analysis, which is governed by the heat transfer equation:

$$\rho C_p \frac{\partial T(x, y, z; t)}{\partial t} - \nabla \cdot (\kappa \nabla T(x, y, z; t)) = \frac{dQ_V}{dt}. \quad (1)$$

Here Q_V is the volumetric heat generated by the absorbed beam, T the temperature, t the time, C_p the specific heat capacity, κ the thermal conductivity, and ρ the mass density. Note that the thermal diffusivity $\alpha = \kappa / \rho C_p$. The volumetric heat can be well approximated by

$$Q_V(\mathbf{r}, t) = \mu_a I(\mathbf{r}, t) / \tau_p, \quad (2)$$

with μ_a the absorption coefficient, τ_p the pulse duration, and I the beam power density (W/cm^2).

The initial condition for Eq. (1) is:

$$T(x, y, z; t_0) = T_\infty, \quad (3)$$

where T_∞ is the ambient air temperature. The surface heat loss (flux, q) due to surface emission by convection is determined by:

$$q_{\text{conv}} = h^*(T_{\text{surf}} - T_\infty), \quad (4)$$

where T_{surf} is the surface temperature and h^* the convective heat transfer coefficient.

Laser Energy Deposition

In this brief study we assume the laser beam has a circular and Gaussian distribution:

$$p(r) = p_0 \exp \left[-2 \left(\frac{r}{k_G w / 2} \right)^2 \right], \quad (5)$$

when its scanning speed $v = 0$. Here $p(r)$ is laser powder density (W/cm^2) as a function of r , the distance from the laser center on the metal surface. k_G is the Gaussian parameter, and its default value is 0.6 in ALE3D so that at the edge ($r = w/2$, with w the width of laser as defined in ALE3D), $p \approx 0.0039 p_0$. The beam peak power density p_0 is:

$$p_0 = \frac{4 \ln(2)}{\pi} \frac{P}{FWHM^2} = 0.88254 \frac{P}{FWHM^2}, \quad (6)$$

where P is the total power, $FWHM$ is the full width at half maximum:

$$FWHM = \sqrt{\ln(2) / 2} k_G w = 0.5887 k_G w. \quad (7)$$

When the scanning speed $v \neq 0$, the power density distribution is:

$$p(x, z, t) = p_0 \exp \left(-\frac{x^2}{2\sigma^2} - \frac{(z - vt)^2}{2\sigma^2} \right), \quad (8)$$

assuming laser is scanning along the z -axis. Here the beam distribution parameter

$$\sigma = k_G w / 4 = FWHM / 2\sqrt{\ln(2)} = FWHM / 2.355. \quad (9)$$

As the beam spot travels on the work plane along the z -axis, the incident energy along the transverse direction (x -axis) is calculated as

$$q_0(x) = \int_{-\infty}^{\infty} p(x, 0, t) dt = q_0 \exp\left(-\frac{x^2}{2\sigma^2}\right). \quad (10)$$

The peak incident fluence (J/cm^2)

$$q_0 = \frac{1}{\sqrt{2\pi}} \frac{P}{\sigma v} = 0.9394 \frac{P}{FWHM \cdot v}. \quad (11)$$

Table I: Summary of laser power P , the full width at the half maximum ($FWHM$), peak power density p_0 , scanning speed v , peak incident fluence q_0 , and the scanning characteristic time ($\tau = FWHM/v$), as used in our ALE3D simulations.

P (W)	$FWHM$ (μm)	p_0 (MW/ cm^2)	v (cm/s)	q_0 (J/cm^2)	τ (μs)
22.5	50	0.794	15	282	333
45	60	1.10	30	235	200
92	54	2.78	38	421	142

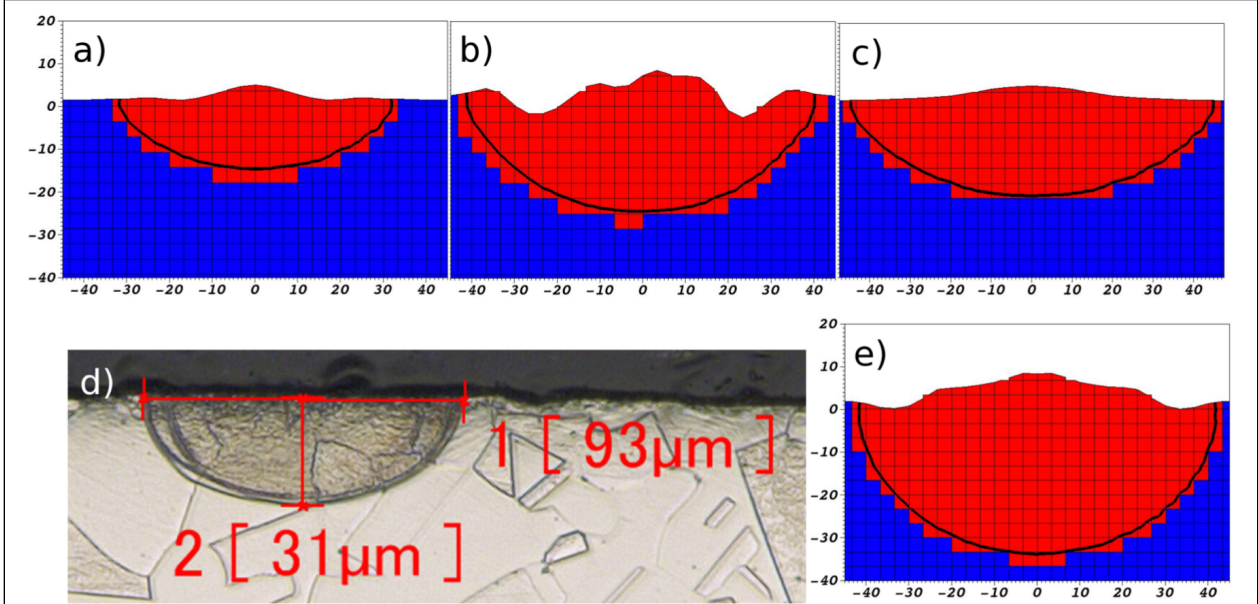


Figure 1. Cross-section micrographs of laser tracks on stainless steel plates. [1] All length units are in μm . The laser absorptivity is 0.44 for (a) ($P = 22.5$ W, $FWHM = 50$ μm , $v = 15$ cm/s), (b) ($P = 22.5$ W, $FWHM = 50$ μm , $v = 30$ cm/s), (c) ($P = 45$ W, $FWHM = 60$ μm , $v = 30$ cm/s) and 0.33 in (e) ($P = 92$ W, $FWHM = 54$ μm , $v = 38$ cm/s). The zones in red indicate a liquid melt, with the melting curve in black with $T = 1700$ K. (d) plots the measured melting hole with the laser power of 92 W, $FWHM$ of 54 μm , and the scanning speed of 38 cm/s.

Thermal and Optical Properties of Stainless Steel

We set the melting point of stainless steel (316L) at 1700 K, the thermal conductivity 20 W/mK, and the thermal capacity 0.5 J/gK. Optical properties of stainless steel depend strongly on sample size and surface

finish. We assumed absorptivity of 44% and 33%, in order to compare results with those obtained from previous ALE3D simulations, as illustrated in Fig. 1.

The optical extinction coefficient, β , for bulk stain steel is set to $7.53 \times 10^5 \text{ cm}^{-1}$, based on experimental estimation. Beam extinction coefficient in metal powder materials is estimated as: [5, 6]

$$\beta = \frac{3}{2} \frac{1 - \varepsilon}{\varepsilon} \frac{1}{d}, \quad (12)$$

which is essentially independent of their bulk values (normally in a range of 10^5 to 10^8 cm^{-1}), when the powder particle size (d) is less than 100 μm . Here ε is the powder porosity. Rombouts and Froyen measured light extinction in metallic power beds using a light-transmission technique at a wavelength of 540 nm, finding that $\beta \approx 500 \text{ cm}^{-1}$ for stainless steel powder with $d = 57 \mu\text{m}$ and a typical porosity of 0.4, in good agreement with Eq. (12). In our ALE3D simulations we used $\beta = 7.53 \times 10^5, 7.53 \times 10^4, 6000, 500 \text{ cm}^{-1}$, to study the dependence of melting on the optical extinction parameter.

Technical Nitty-Gritties

- (1) We set the minimum grid size to 1 μm near the on-spot ($v = 0$) laser region in 2D simulations, while the minimum grid size is 2 μm in our 3D simulations when laser is scanning.
- (2) In 2D simulation for a circular laser, the axis symmetry must be turned on. 2D axis-symmetry always assumes that the simulated system rotates around the x -axis.
- (3) In our 2D and 3D simulations, the strong loading near the axis will excite a fictitious electromagnetic mode in the default hydrodynamic integration mode, causing the system to crash. We changed the integration mode in the HYDRO block by setting


```
elem_integration 2
hgmodel 2
```
- (4) Since ALE3D does not have the physics of laser-plasma interactions, the absorption tables for solid materials are relatively unsophisticated and we can set the values by the following thumb rules:
 - a. Based on the zone size (depth) at the surface, set the mean free path to be a zone or two; for instance, for millimeter zoning, set `absorb = 10 cm-1` if no experimental data available.
 - b. Go up and down in density space a few orders of magnitude and keep the absorption length consistent; for instance, at 10% density, `absorb = 1 cm-1` if it is 10 cm^{-1} at 100% density.
 - c. For a temperature function, there aren't any extra physics can be accounted for, so just keep a wide temperature range of temperature to stay within the table bounds.
- (5) Replacing a laser with an electron beam is relatively straightforward, except that one has to add a row of void zones or some dummy materials to the back side to avoid a bug, if the energy of e-beam is not all absorbed by the material.

3. Results

On-Spot Lasering ($v = 0$)

Fig. 2 summarizes the evolution of the melting of stainless steel by laser with $P = 22.5 \text{ W}$, $FWHM = 50 \mu\text{s}$. Steel surface reaches the melting temperature at around 30 μs . Its width-to-depth ratio of the melted hole decreases gradually from about 10 to around 3, as indicated in Fig. 3(b), until the maximum surface temperature reaches the boiling point of 3100 K at $t = 780 \mu\text{s}$.

Figs. 3(a) and 3(b) demonstrate that for the optical extinction parameter β in the testing range of 7.53×10^5 to 6000 cm^{-1} , the evolution of melt width and melt depth with respect to time (absorbed energy) barely changes—steel starts to melt at t in the range of 30-60 μs and the melt width-to-depth ratio decreases from about 10 to 3 around $t = 800 \mu\text{s}$. However, when β is further reduced to 500 cm^{-1} , the value for stainless

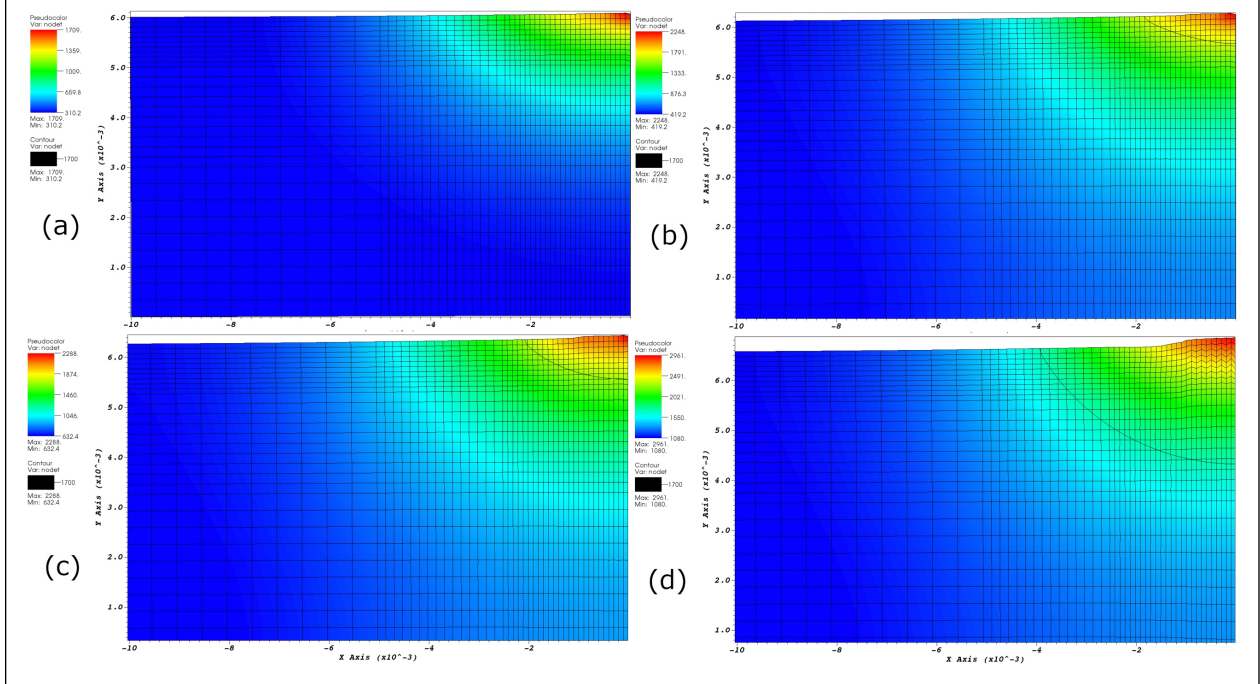


Figure 2. Melting of stainless steel (316L) by a laser beam with $P = 22.5$ W and $FWHM = 50$ μm . In this simulation, optical absorptivity is 0.44 and the extinction coefficient is 7.53×10^5 cm^{-1} . Panels (a), (b), (c) and (d) correspond to time $t = 30, 170, 330$, and 670 μs , respectively, with the maximum temperatures of 1709, 2248, 2288, 2961 K. The black curve indicates the melting surface.

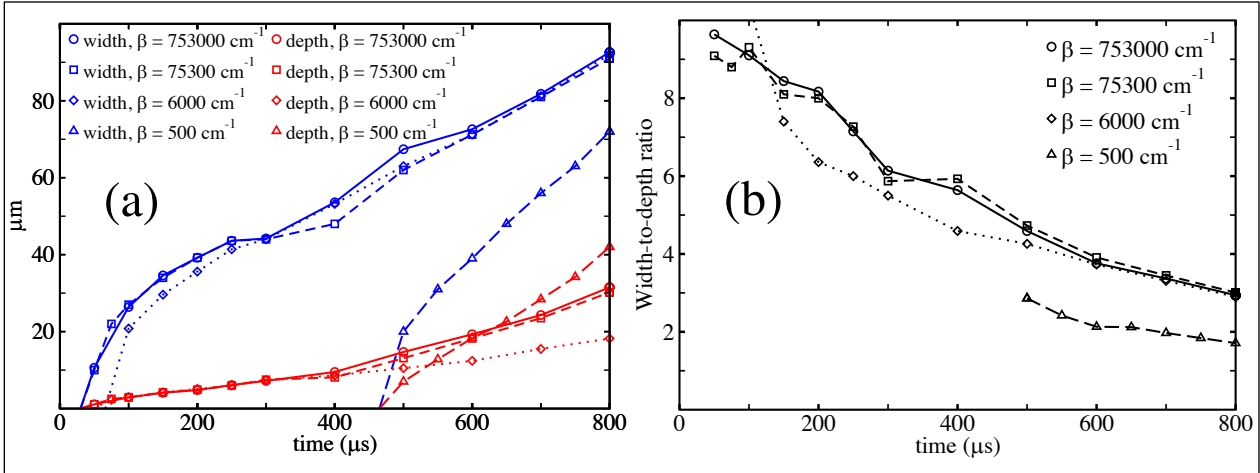
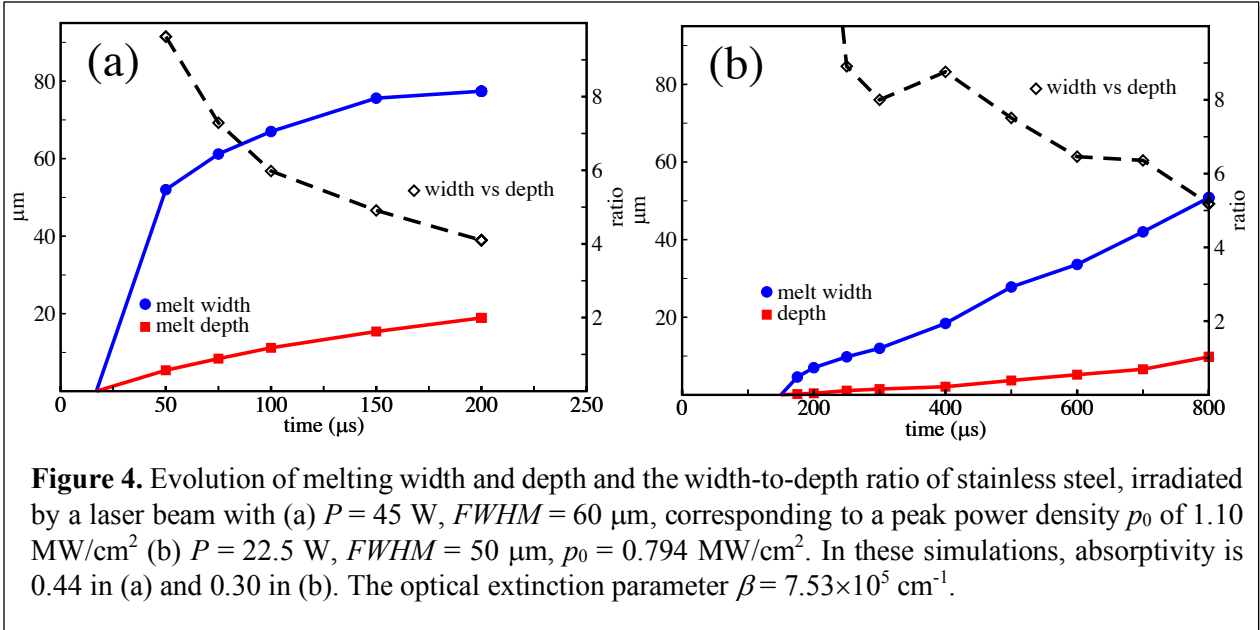


Figure 3. Evolution of melting width and depth (a) and the width-to-depth ratio (b) of stainless steel with various optical extinction parameters β , irradiated by a laser beam with $P = 22.5$ W and $FWHM = 50$ μm , corresponding to a peak power density p_0 of 0.794 MW/cm 2 . In these simulations, absorptivity is 0.44.

steel powder with size of 57 μm , dramatic change in melting occurs: (1) steel starts to melt at $t = 465$ μs ; (2) its width-to-depth ratio is much lower, decreasing from initial value of 2.9 to about 2 at $t = 670$ μs . These can be understood by more penetration of laser into steel with smaller extinction parameter.

We also examined the effects of power density and optical absorptivity on melting. Comparing Fig. 3 with Fig. 4(a), one finds that increasing p_0 from 0.794 MW/cm 2 ($P = 22.5$ W, $FWHM = 50$ μm) to 1.10 MW/cm 2



($P = 45$ W, $FWHM = 60$ μm) (1) reduces the irradiation time ($t = 17$ μs) required to melt steel; (2) causes both melt width and depth to increase much faster; (3) reaches the boiling point much quicker ($t = 190$ μs). On the other hand, when absorptivity is reduced from 0.44 to 0.30 , (1) melting requires 150 μs of irradiation ($P = 22.5$ W, $FWHM = 50$ μm) and (2) both melt width and depth become significantly smaller.

Laser Scanning ($v \neq 0$)

Fig. 5 summarizes the temperature distribution in stainless steel during the heating and melting processes by laser beams with scanning speed $v = 15$ cm and 30 cm. Compared with on-spot lasering ($v = 0$), a travelling laser with the same power parameters (1) requires longer time to melt steel while (2) the melted width and depth are reduced. Fig. 6 compares the melt holes for three laser beams. Note that these simulations haven't reach the equilibrium state yet, and the final configurations in Figs. 6(a), 6(b), and 6(c) are expected to match those in Figs. 1(a), 1(c) and 1(e), respectively.

These 3D simulations are much more time consuming than 2D. Currently the smallest grid size is set to be 2 μm , which is not sufficient; however, each simulation requires about 10 days for 8 cores to reach 100 μs . We need to reduce the minimum grid size to 1 μm ; otherwise the simulations will crash before reaching the equilibrium configurations. Large scale national computation facilities are in need for ALE3D simulations of powder bed fusion by electron beam.

4. Conclusions and Future Work

The main goal of this study is to demonstrate that we have the ability of carrying reliable ALE3D simulations of energy beam heating and melting metals. Our present FEM of laser interaction with bulk stainless steel paves the way for e-beam processing metallic powder materials, though the enormous computational overheads demand national computation facilities and the complexity involved such as keyhole formation, requires additional model development.

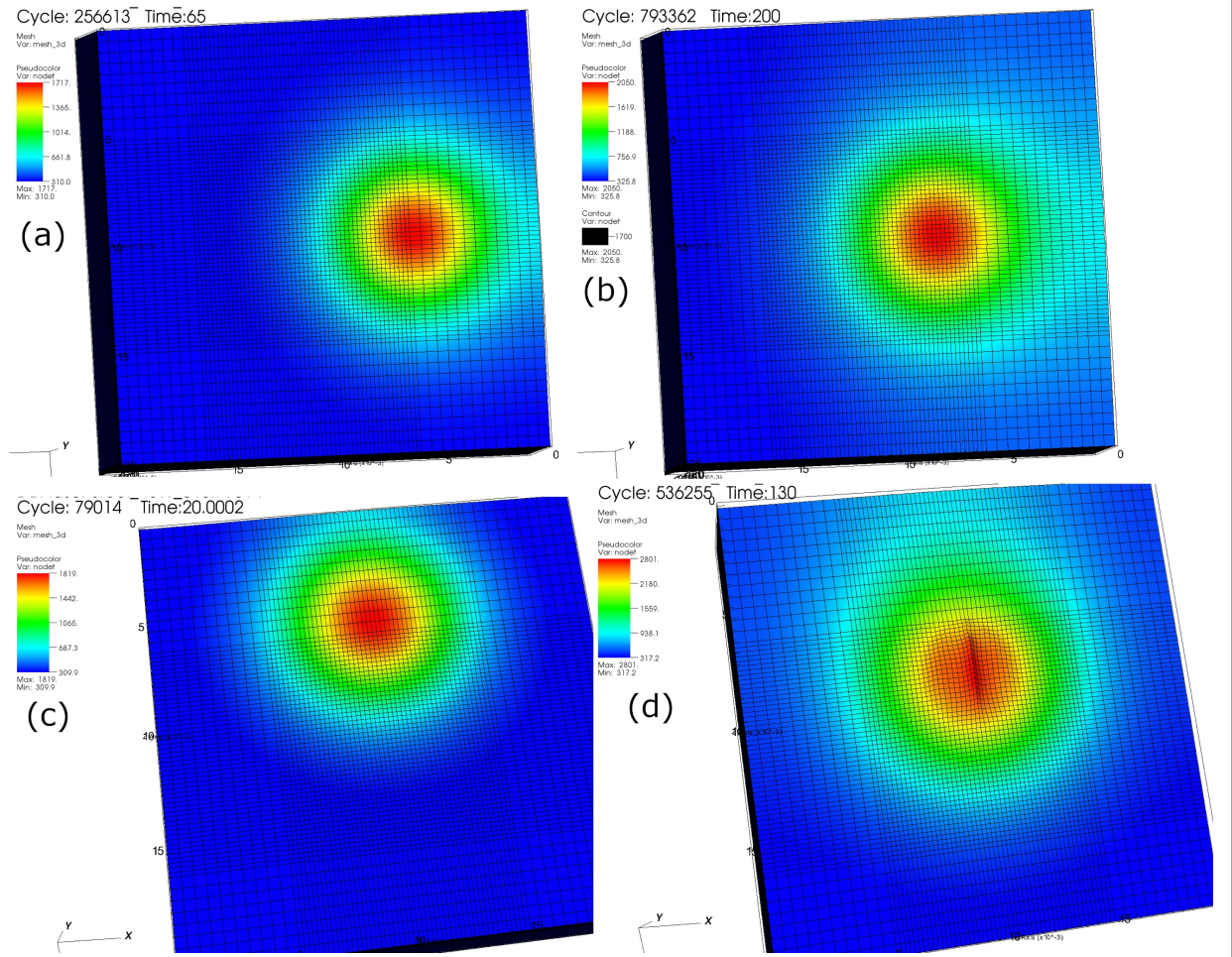


Figure 5. Temperature distribution of stainless steel heated by a laser beam with $P = 22.5 \text{ W}$, $FWHM = 50 \mu\text{m}$, scanning speed of 15 cm/s , at (a) $t = 65 \mu\text{s}$ and (b) $t = 200 \mu\text{s}$. (c) and (d) shows the temperature distribution for $P = 45 \text{ W}$, $FWHM = 60 \mu\text{m}$, $v = 30 \text{ cm/s}$, at $t = 20 \mu\text{s}$ and $130 \mu\text{s}$, respectively. In these simulations, optical absorptivity is 0.44 and the extinction coefficient is $7.53 \times 10^5 \text{ cm}^{-1}$.

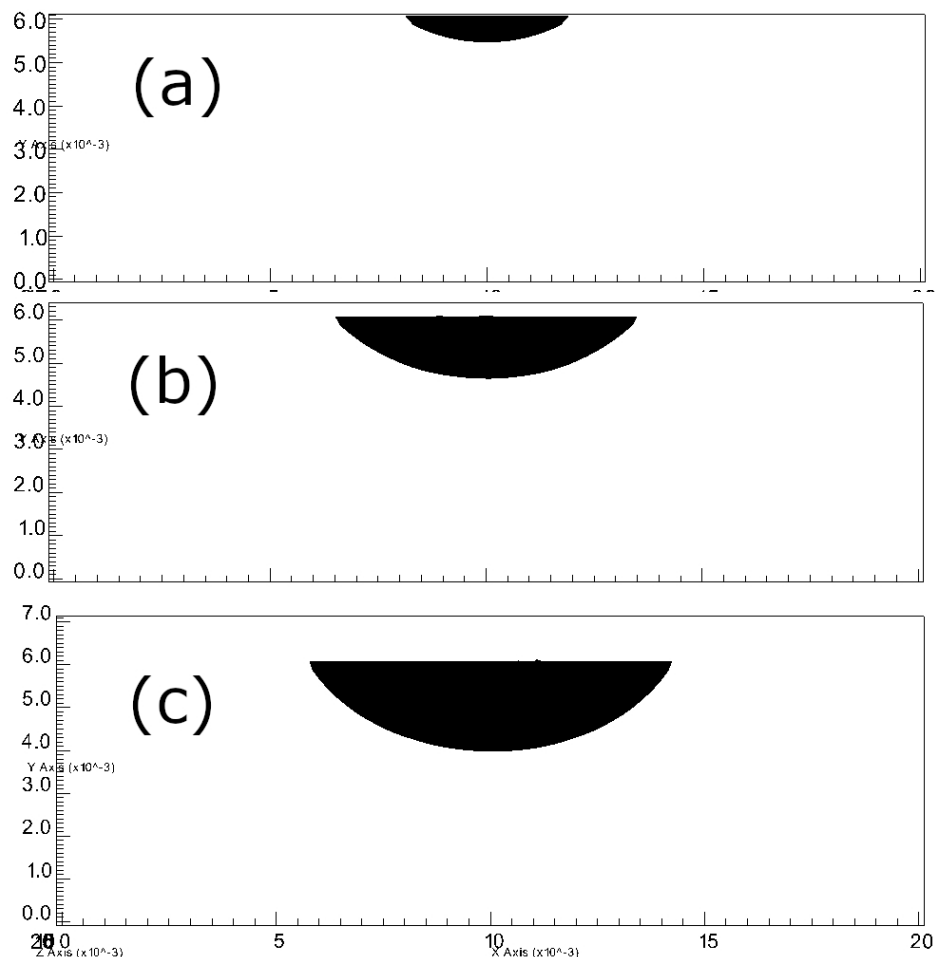


Figure 6. Melting hole cross sections of stainless steel by laser beams. (a) $P = 22.5$ W, $FWHM = 50$ μm , $t = 200$ μs , absorptivity = 0.44; (b) $P = 45$ W, $FWHM = 60$ μm , $t = 130$ μs , absorptivity = 0.44; (c) $P = 92$ W, $FWHM = 54$ μm , $t = 25$ μs , absorptivity = 0.44. Here $\beta = 7.53 \times 10^5$ cm^{-1} .

References

1. S. A. Khairallah, A. Anderson. Mesoscopic simulation model of selective laser melting of stainless steel powder. *Journal of Materials Processing Technology* **214**(11), 2627-2636 (2014).
2. Kyle Maxey. GE CEO Jeff Immelt on 3D Printing. Engineering.com. 2013.
3. ALE3D: Arbitrary Lagrangian-Eulerian 3D and 2D Multi-Physics Code. Available from: <https://wci.llnl.gov/simulation/computer-codes/ale3d>
4. L. W. Malvern. *Introduction to the Mechanics of a Continuous Medium*. Prentice-Hall: Englewood Cliffs, 1969.
5. M. Rombouts, L. Froyen, A. V. Gusarov, E. H. Bentefour, C. Glorieux. Light extinction in metallic powder beds: Correlation with powder structure. *Journal of Applied Physics* **98**(1), 013533 (2005).
6. A. V. Gusarov, I. Yadroitsev, P. Bertrand, I. Smurov. Model of Radiation and Heat Transfer in Laser-Powder Interaction Zone at Selective Laser Melting. *Journal of Heat Transfer* **131**(7), 072101-072101-072110 (2009).